ACS Sustainable Resource Management

pubs.acs.org/acssrm

Article

Biochar Stability Revealed by FTIR and Machine Learning

Monica A. McCall,* Jonathan S. Watson, Jonathan S. W. Tan, and Mark A. Sephton

Cite This: *ACS Sustainable Resour. Manage.* 2025, 2, 842−852

Read Online

ACCESS | Metrics & More | Article Recommendations | Supporting Information

ABSTRACT: Biochar is a carbon-rich and environmentally recalcitrant material, with strong potential for climate change mitigation. There is a need for rapid and accessible estimations of biochar stability, the resistance to biotic and abiotic degradation in soil. This study builds on previous work by integrating Fourier-transform infrared spectroscopy (FTIR) data with predictive modeling to estimate standard stability indicators: H:C and O:C molar ratios. Lignocellulosic feedstocks were pyrolyzed at highest treatment temperatures (HTT) ranging from 150−700 °C, and all samples achieved H:C < 0.7 and O:C < 0.4 at HTT of 400 °C and above. Several statistical and machine learning models were developed using FTIR spectra. The random forest (RF) models, which incorporated full data preprocessing, yielded the highest accuracy (R^2 = 0.96 for both ratios) when tested on an unseen feedstock. Variable importance analysis identified spectral regions linked to aromaticity and inversely correlated to C−O stretches in cellulose and lignin as key predictors. The findings of this study verify that FTIR data can serve as a rapid and accurate tool for estimating biochar stability.

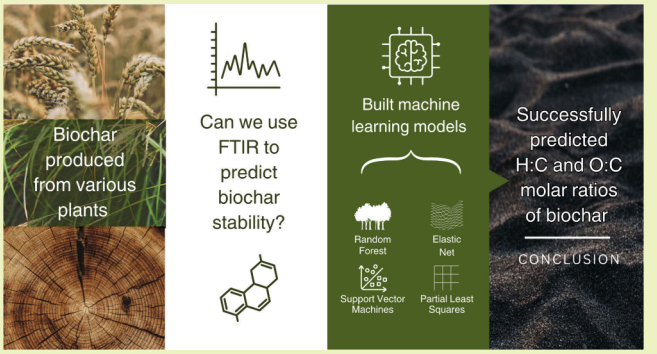

KEYWORDS: *infrared spectroscopy, H:C, O:C, molar ratios, modeling, wood, grass, Random Forest*

INTRODUCTION

With global surface temperatures now surpassing 1.1 °C above preindustrial levels,[1] carbon dioxide removal (CDR) methods are gaining significant momentum. Among these, biochar, a carbon-rich and environmentally recalcitrant material produced from the pyrolysis of biomass,[2] has garnered particular interest, with projected sales exceeding $368 million by 2028.[3] Biochar can sequester 2.5 $GtCO_2$ per year,[3] while improving soil properties such as nutrient availability, soil organic carbon, crop yields, and water retention.[4] As its role in climate mitigation and soil amelioration grows, efficient biochar characterization and monitoring techniques must evolve at a pace.

Machine learning, an artificial intelligence application that predicts outcomes without rigorous programming,[5] is increasingly used across scientific fields,[6] including biochar research.[7] By replacing the need for otherwise lengthy and expensive laboratory experiments, machine learning facilitates more time- and cost-effective analyses.[8] Additionally, accessible coding packages now enable custom-built models, particularly useful for large, complex, and high-dimensional datasets. Several studies have applied machine learning to predict biochar characteristics using known physiochemical properties and pyrolysis conditions,[9] including predicting heavy metal adsorption,[10] specific surface area, pore volume,[11] and elemental composition.[12] Others have used ^{13}C nuclear magnetic resonance spectroscopy (NMR) data alone to estimate the biochar composition.[13]

Fourier-transform infrared spectroscopy (FTIR) is a rapid, non-destructive, and cost-effective method for detecting chemical functional groups in a sample,[14,15] rendering it ideal for biochar characterization when production details are unknown, such as in artisanal biochar produced in rural areas. FTIR's ease of data acquisition and information richness render it well-suited for predictive modeling, as its spectra offer abundant data for machine learning.[16] Despite the advantages of both machine learning and FTIR, their combined applications in biochar research are limited. Wehrle et al.[17] used support vector machines (SVM) and FTIR to characterize carbon and nitrogen in biochar-based soil amendments. Other studies have paired FTIR with simpler models to predict cation exchange capacity[18] and other properties of biochar-based fertilizers.[19] Sajdak et al.[20] achieved 92−99% accuracy in classifying biomass sources of biochars using FTIR spectra, but there still remains few studies that leverage advanced machine learning techniques for FTIR data.

A notably valuable application of these methods lies in predicting biochar stability or the resistance to biotic and abiotic degradation.[21] In order to be certified by regulatory

Received: February 21, 2025
Revised: April 9, 2025
Accepted: April 11, 2025
Published: April 29, 2025

Table 1. Chemical Composition of Each Raw Feedstock, as Found in the Literature

Feedstock	Type	Photosynthetic pathway	Cellulose (%)	Hemicellulose (%)	Lignin (%)	Ash (%)	Extractives (%)	Reference
Barley Straw (BS)	Grass	C3	34-45	28-36	16-22	4-9	3-8	27−31
Rice Husk (RH)	Grass	C3	25-35	18-26	7-31	10-24	5-12	32−35
Chestnut Wood (CW)	Hardwood	C3	32-47	18	18-33	0.1-1.2	6-16	36−38
Eucalyptus Bark (EB)	Hardwood	C3	23-42	19-23	16-45	5-14	1-10	39−43
Pine Bark (PB)	Softwood	C3	17-28	12-23	41-51	1-4.5	4-17	44−47
Miscanthus Grass (MG)	Grass	C4	33-50	21-35	17-28	1-8	9	48−50

bodies, biochar stability is evaluated by its molar ratios of H:C and O:C. Only biochar achieving H:C < 0.7 and O:C < 0.4 is approved for certification.[22,23] The current standard for determining these ratios is elemental analysis, a process that is lengthy, expensive, and destructive and requires technical expertise. Conversely, FTIR spectroscopy offers a faster and more accessible alternative for producers and certifiers alike. Previous proof-of-concept research demonstrated that simple statistical models could predict H:C and O:C ratios with high accuracy (R^2 > 0.98) for a single feedstock.[24] However, to the best of our knowledge, no other studies have explored the use of machine learning to ascertain stability information from FTIR data. This study aims to bridge that gap by applying machine learning techniques to FTIR spectra, enabling rapid and accurate stability predictions.

MATERIALS AND METHODS

Feedstocks. Feedstocks included three species of grass: barley straw (BS), miscanthus grass stems (MG), and rice husk (RH), and three species of wood: chestnut wood (CW), eucalyptus bark (EB), and pine bark (PB). Selected woods included both hard and softwood as well as bark. Lignocellulosic feedstocks were chosen for their popularity in biochar production.[25] Additionally, one C4 plant (MG) was included. All feedstocks are on the EBC's list of permissible biomasses for biochar production.[26] Lastly, these feedstocks represent a range of chemical compositions, summarized in Table 1. Briefly, wood feedstocks are characterized by higher lignin content, whereas greater levels of the biopolymers cellulose and hemicellulose are found in the grasses. Rice husk, known for its silica content, generates a high amount of ash. Extractives, the nonstructural chemical compounds in plants, were in similar ranges across all feedstocks.

Biochar Production. All feedstocks were pyrolyzed in a Carbolite Gero tube furnace at 5 °C/min heating and cooling rates under an inert N_2 atmosphere (1 L/min flow rate). The highest treatment temperature (HTT) ranged from 150−700 °C in 100 °C increments, with samples held at HTT for 30 min. Because significant compositional changes of biochars arise between 250 and 350 °C,[24] samples were pyrolyzed at these temperatures as well. BS biochar was additionally produced at 150, 450, 550, and 650 °C. Resultant biochars were then weighed and homogenized to ensure sample homogeneity in the FTIR analysis.

FTIR Specifications. All biochar and feedstocks were analyzed using attenuated total reflectance FTIR (ATR-FTIR) on a Nicolet 5700 Spectrometer. Samples were run in triplicates of 128 scans, in the mid-infrared region of 3700−550 cm^{-1} at 4 cm^{-1} resolution. Spectra were baseline corrected using Spectragryph software using the advanced adaptive baselining method.[51]

Elemental Analysis. Elemental analysis was conducted by Sercon Analytical Ltd. on a Europa Scientific Elemental Analyzer coupled with Isotope Ratio Mass Spectrometry (EA-IRMS). Twenty percent of samples were duplicated and averaged, and the instrument has a relative standard deviation of 2%.

Model Development and Evaluation. *Data Partitioning.* Model development and analysis were conducted in R (version 3.4.0) using the caret package.[52] The predictor variables for the models were the absorbance values at each particular wavenumber in the FTIR spectra. The response variables were H:C and O:C respectively, chosen for their use in the biochar certification process. FTIR data was divided into training (∼80%) and testing (∼20%) sets. The training set included spectra from RH-, CW-, EB-, PB-, and MG-derived biochars, while the test set comprised only BS-derived biochars. The test set contained HTTs absent from the training set but within a similar range, allowing for evaluation of model performance on unseen feedstocks and temperatures.

Preprocessing. Data preprocessing, a collection of techniques used to refine data quality, is an integral step for improving prediction accuracy in machine learning.[53] Normalization, a common practice in FTIR analysis, was performed using a min-max method,[54] where each spectrum was transformed such that the highest absorbance peak was equivalent to 1. Scaling involved standardizing each predictor variable by dividing it by the standard deviation across all samples. Lastly, principal component analysis (PCA), a dimensionality reduction technique, was applied to address the large number of predictor variables by transforming them into uncorrelated principal components (PCs).[52] The PCA threshold was set to 95%, ensuring that only the most relevant PCs that cumulatively explain 95% of the variance in the predictors were retained. Models were developed by using different preprocessing combinations to identify optimal techniques.

Model Training and Hyperparameter Tuning. To maximize performance while addressing the limited number of observations, K-fold cross-validation was employed in model training.[55] This involved splitting the training data into K = 10 equal "folds", where K-1 folds are used to predict the left-out fold as a temporary test set, allowing for the model to be trained and applied to K different datasets.[56] Hyperparameter tuning was performed for each model and preprocessing combination using a grid search approach. This involved setting up an initial grid space and step size, which was then continuously refined to focus on optimal ranges and increase granularity.[57] The grid search was completed when perturbations in hyperparameters resulted in negligible improvements in resampling performance (change in root mean square error (ΔRMSE) < 0.01 across all 10 cross-validated resamples). To ensure reproducible results, the set.seed() function was used to hold the composition of the folds constant throughout model training.[52]

Various model algorithms, both statistical and machine learning, were tested separately for the H:C and O:C predictions. A supervised statistical method, partial-least-squares regression (PLSR), was chosen for its prior success in other FTIR related studies.[18,19] Elastic net regression, a variable selection and regularization model, is useful when the number of observations is smaller than the number of predictors.[58] Random Forest (RF) uses a decision tree algorithm which utilizes bootstrap aggregation and randomization of predictors to create many decision trees and achieve highly accurate predictions.[59] Lastly, support vector machine (SVM) models generalize well to unseen data by maximizing the margin between data points and decision boundaries.[60] The machine learning algorithms chosen are widely used for regression analysis in other fields, are simple to implement and tune, do not require excessive processing power, and are relatively easy to interpret.

Model Evaluation. Model performance was assessed by comparing the cross-validated resampling results using the coefficient of determination (R^2) and RMSE as evaluation metrics. Following cross-validation, the final models were applied to the unseen test set to predict the H:C and O:C ratios. The variable importance of the

https://doi.org/10.1021/acssusresmgt.5c00104
ACS Sustainable Resour. Manage. 2025, 2, 842−852

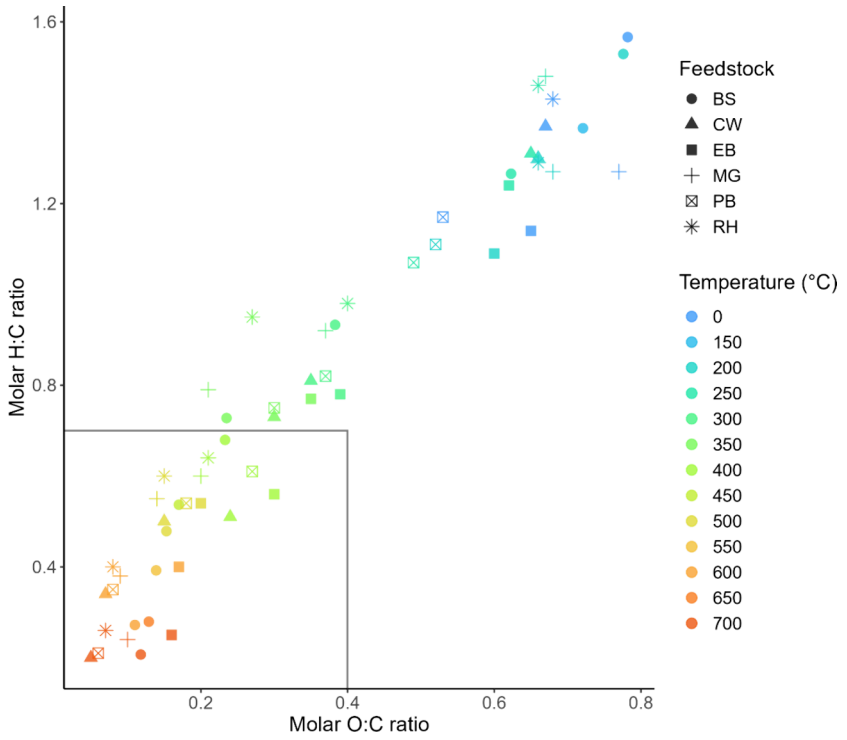

Figure 1. Van Krevelen diagram of both H:C and O:C molar ratios of biomass and biochars produced from the various feedstocks over a range of pyrolysis HTT. The black rectangle represents the ratios determined by EBC and IBI to certify biochar as suitable for soil amendment.[22,23]

best-performing models (as determined by R^2 and RMSE) was further explored to identify the regions of the FTIR spectra most influential in driving model predictions.

RESULTS AND DISCUSSION

Elemental Analysis. The van Krevelen diagram in Figure 1 illustrates the relationship between molar H:C and O:C ratios across all feedstocks and biochars. There is a clear trend of reduction in both ratios with increasing temperature. The unpyrolyzed feedstocks have an average H:C and O:C ratio of 1.32 ± 0.15 and 0.68 ± 0.09 respectively, demonstrating large variability in the chemical composition of the starting materials. In contrast, at the HTT of 700 °C the H:C ratio converges to an average of 0.23 ± 0.02, and the O:C ratio converges to an average of 0.09 ± 0.04 across feedstocks. This indicates that while initial composition has a substantial effect on both molar ratios, as HTT increases, the ratios become more dependent on temperature than starting material.[61,62] Some feedstocks began at relatively lower ratios, reflective of their starting compositions. For example, the unheated lignin-rich PB had an H:C value of 1.17 and an O:C value of 0.53, indicating it had lower ratios than those of cellulose-rich BS pyrolyzed to 250 °C. However, the two have nearly identical H:C ratios at 700 °C, implying that BS underwent a more gradual degradation rate compared to PB. All biochars produced at HTT ≥ 400 °C met the criteria determined by EBC to certify biochar as suitable for soil amendment[22,23] regardless of starting material. CW biochar produced at 700 °C had the lowest ratios of all the samples (H:C = 0.2, O:C = 0.05), with an estimated carbon storage of 574 g/kg after 100 years in soil, as determined by the IBI carbon storage classification tool.[63] Lastly, the figure suggests a high correlation between O:C and H:C. However, we caution the use of this relationship and advise it may only be used as an estimation limited to lignocellulosic feedstocks, as the literature shows examples where non-lignocellulosic feedstocks do not display the same linear correlation.[64]

FTIR Spectra. The fingerprint region of the FTIR Spectra of all biochar samples and starting materials can be found in Figure 2. Spectra containing higher wavenumbers can be found in the Supporting Information.

The common peaks and their assignments are summarized in Table 2. For all feedstocks, peaks around 1700 cm^{-1} are indicative of acetyl, ester, carboxyl groups in hemicellulose and lignin[65−67] and decrease with temperature. Aromatic skeletal vibrations at ∼1510 cm^{-1} are present at low HTT but are removed around 200−300 °C for the grass-derived biochars and after 400 °C in the woods. The presence of the C−O stretch at 1030 cm^{-1} dominates the spectra of the unheated biomasses and dampens with temperature across all samples except for RH, where this peak remains prominent at 700 °C. As RH is recognized for its high silica content,[35] this is likely due to a signal of the Si−O−Si stretch at the same wavenumber, corroborated by an additional Si−O−Si bend present at 815−790 cm^{-1}.[68] Peaks corresponding to aromatic C−H bends began to form particularly from 400−600 °C, signaling the formation of stable aromatic rings.[69] However, peaks in this region diminish in most feedstocks at 700 °C as the high HTT drives off the majority of hydrogen, leaving only graphitic carbon remaining.[70] The one exception is EB-derived biochar, where the out-of-plane C−H bend peak at 785 cm^{-1} is present from 250−400 °C and degraded above 400 °C. This could be attributed to condensed tannins[71] or polyphenolic compounds such as the flavonoid quercetin, which has a characteristic peak in this region and is present in eucalyptus.[72] BS and EB are also the only spectra to retain a C−H bend peak around 1430 cm^{-1} at 700 °C.

https://doi.org/10.1021/acssusresmgt.5c00104
ACS Sustainable Resour. Manage. 2025, 2, 842−852

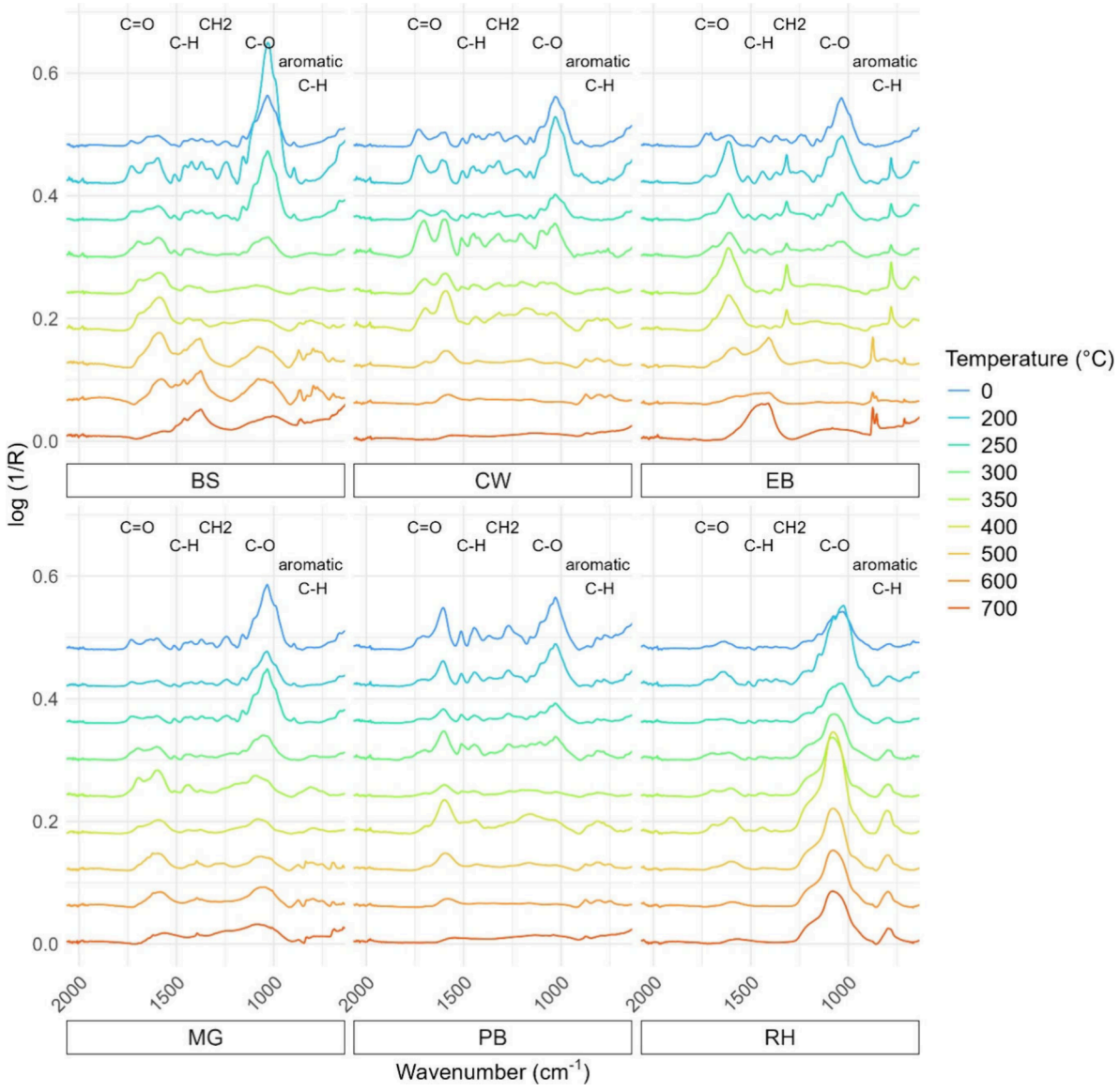

Figure 2. ATR-FTIR spectra of all biochars and starting materials; each spectrum is an average of triplicates for illustrative simplicity and is displayed on a common, offset *y*-axis. HTT is denoted by color, and common peak assignments are noted above their respective peaks.

Table 2. Common Peaks in the ATR-FTIR Spectra of All Biochars with Chemical Assignments[a]

Peak (cm^{-1})	Chemical assignment	Reference
1750–1650	C═O stretch	76
1595–1512	aromatic skeletal vibration	74, 77, 78
1462–1316	C–H bend and CH_2 wag + O–H bend vibrations	74, 76–79
1247–1030	C–O stretch in lignin + cellulose	74, 76, 78–80
870–680	aromatic C–H bend	69, 81, 82
815–790	Si–O–Si bend	68
750–650	C–OH out of plane bend	79

[a]More detailed assignments related to the biopolymers lignin and cellulose have been previously reported.[24]

Differences in hardwoods and softwoods were identifiable. PB, a softwood, contains more G-units and displayed prominent G-unit specific peaks such as the C–O stretch at 1267 cm^{-1} and aromatic C–H bend at 813 cm^{-1}.[73] Meanwhile, both EB and CW, hardwoods, contain a mix of G- and S-units and exhibited more S-unit characteristics peaks, such as the C–O stretch located at 1315 cm^{-1}.[74] Other studies have leveraged this difference and predicted hardwood and softwood contents using FTIR and statistical models.[75]

Modeling. *Cross-Validation.* To optimize model performance, each model and preprocessing combination were treated as individual models, where hyperparameters were tuned using grid search, a common method for hyperparameter optimization.[83] The results of hyperparameter tuning and selection for each model are summarized in Table S3 in the Supporting Information. A summary of the R^2 and RMSE values of cross-validated model training can be found in Figure 3.

During cross-validation, 50% of the H:C models had a mean R^2 above 0.9, though preprocessing caused mixed results in model performance. For elastic net and PLSR models, preprocessing improved R^2 values, aside from scaling in PLSR. For SVM and RF models, normalizing and scaling

https://doi.org/10.1021/acssusresmgt.5c00104
ACS Sustainable Resour. Manage. 2025, 2, 842–852

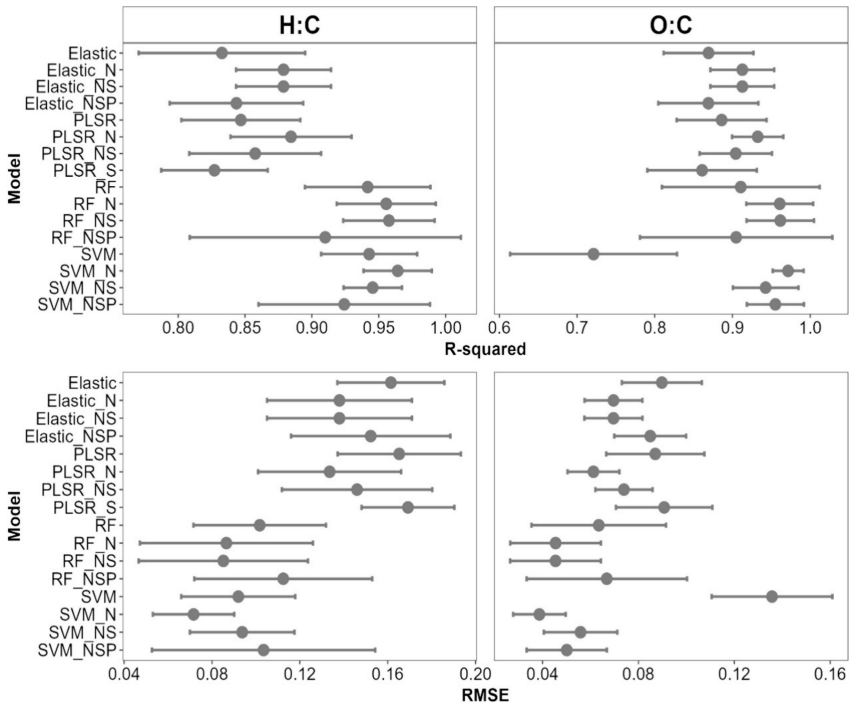

Figure 3. Model comparisons of R^2 and RMSE for both predicted H:C and O:C ratios on training data. The dot signifies the mean of the cross-validated resamples, and the error bars display the standard deviation. Preprocessing steps are abbreviated to N (normalized), S (scaled), NS (normalized and scaled), and NSP (normalized, scaled, and PCA).

improved predictions, but adding PCA generated more variability in the cross-validated resamples, as demonstrated by wider error bars. For the H:C model, the SVM_N model performed most optimally (mean R^2 = 0.96 ± 0.02), followed by the RF_N and RF_NS models (both mean R^2 = 0.96 ± 0.04). The SVM_N training model also had the lowest mean RMSE of 0.04 ± 0.02.

Sixty-nine percent of O:C models attained mean R^2 values above 0.9. SVM_N performed best with a mean R^2 = 0.97 ± 0.02 and RMSE of 0.04 ± 0.01. This model also exhibited the smallest standard deviation across all metrics, signifying consistency in the cross-validated resamples. Like the H:C models, the RF_N and RF_NS models also performed well, both achieving a mean R^2 = 0.96 ± 0.04. The SVM model without preprocessing performed the poorest (mean R^2 = 0.72 ± 0.1 and RMSE of 0.13 ± 0.03), potentially due to overfitting to noise or irrelevant features in the spectra.

Predictions on Test Data. After tuning and training were complete, the models were then deployed on the test data, consisting of FTIR spectra from BS biochar. Scatter plots of the actual molar ratios against predicted ratios are illustrated in Figure 4.

For the H:C prediction on test data, models that used elastic net algorithms and PLSR algorithms achieved roughly similar results, with mean R^2 values of 0.71 ± 0.03 and 0.72 ± 0.05 respectively. Models using RF and SVM algorithms produced relatively more accurate results with mean R^2 = 0.83 ± 0.1 and 0.81 ± 0.05 respectively. The best-performing individual model for H:C was the RF with full preprocessing (RF_NSP), achieving R^2 = 0.96 and RMSE of 0.15. The same model was also most optimal for the O:C predictions, with R^2 = 0.96 and RMSE of 0.08. Because the R^2 value of RF_NSP was the same for H:C and O:C predictions, this signifies that the model was able to equally assess hydrogen and oxygen content information from the FTIR data. The poorest performing algorithm for the O:C predictions was the elastic net, with mean R^2 = 0.70 ± 0.02, and slightly better was the PLSR, with a mean R^2 of 0.72 ± 0.05. SVM models performed worse on O:C predictions than H:C, with mean R^2 = 0 .78 ± 0.19, having the greatest variability due to preprocessing differences across them. Once again, RF models achieved the highest predictive accuracy with a mean R^2 = 0.89 ± 0.07.

These results indicate that RF is best suited for FTIR data for both H:C and O:C predictions. However, preprocessing can have significant effects, as RF predictions on H:C improved by 35% when implementing the normalization, scaling, and PCA steps compared to the non-preprocessed version. Although improvements on the O:C predictions between unprocessed and RF_NSP results were negligible, it is advised that preprocessing be used on a case-by-case basis. Most models exhibited weaker performance on test data than train data (Figure 3), indicated by lower testing R^2 (R^2_{test}) compared to the R^2 of the same model during training (R^2_{train}). This is a common trend, as a meta-review of biochar machine learning studies found R^2_{test} to be lower than R^2_{train} in nearly all cases.[9] This discrepancy is likely due to overfitting, where the model learns the training data too well and fails to generalize to unseen test data.[84] Figure 4 also reveals that extreme values for molar ratios, particularly H:C values beyond the range of 0.6–1.4 or O:C values outside 0.2–0.7, were more difficult for the models to predict. In FTIR spectra of biochars with low molar ratios (Figure 2), most peaks have been removed or dampened, which is likely why the models have more trouble in this range of ratios.

Though previous work[24] established that stability data could be accurately predicted from FTIR spectra using one feedstock, the results here indicate that molar ratio predictions can be

https://doi.org/10.1021/acssusresmgt.5c00104
ACS Sustainable Resour. Manage. 2025, 2, 842–852

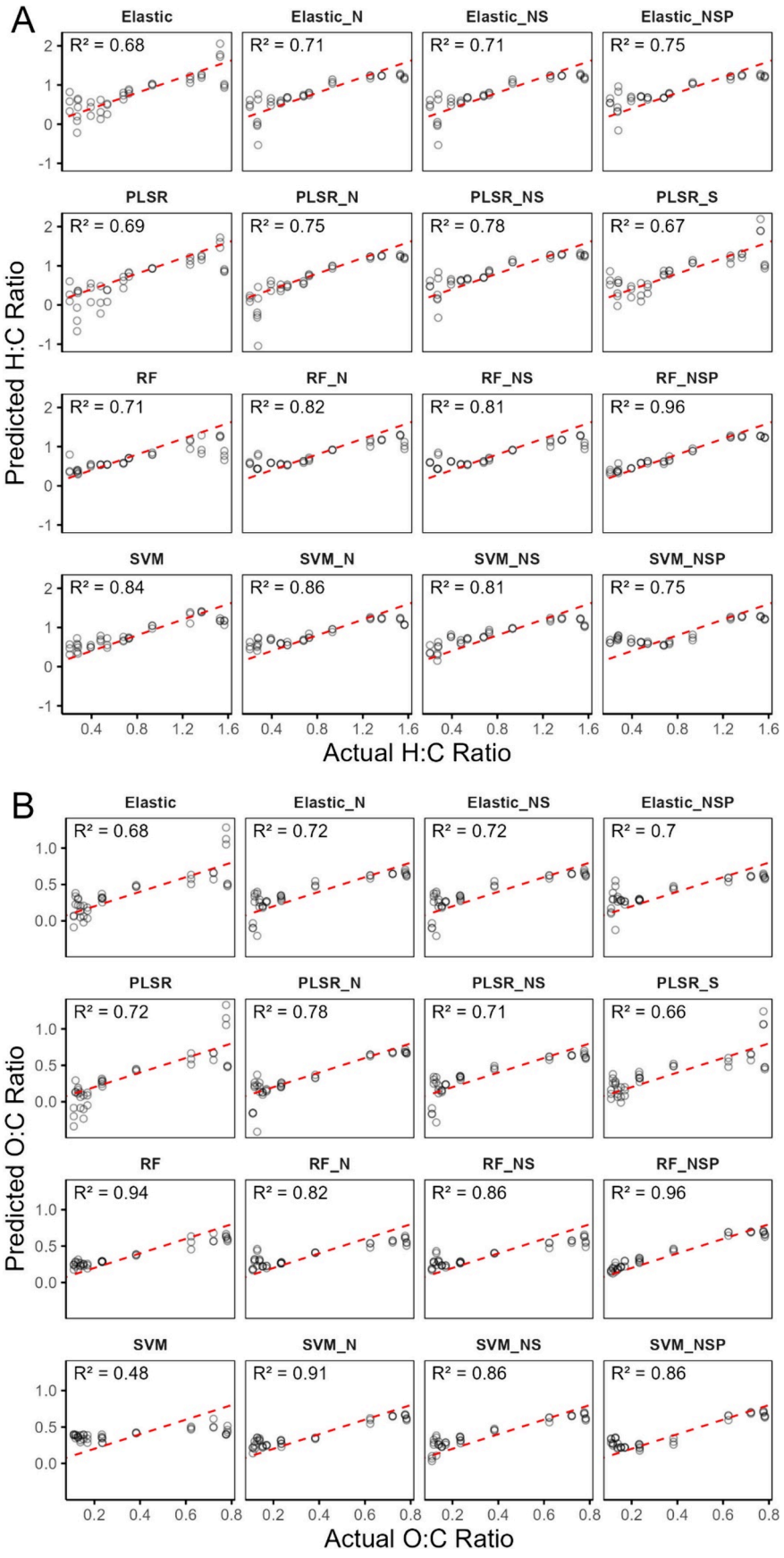

Figure 4. Model predictions of H:C and O:C molar ratios vs actual values on unseen test data, which comprises a new feedstock (BS) and temperature treatments. Preprocessing steps are abbreviated to N (normalized), S (scaled), NS (normalized and scaled), and NSP (normalized, scaled, and PCA).

https://doi.org/10.1021/acssusresmgt.5c00104
ACS Sustainable Resour. Manage. 2025, 2, 842−852

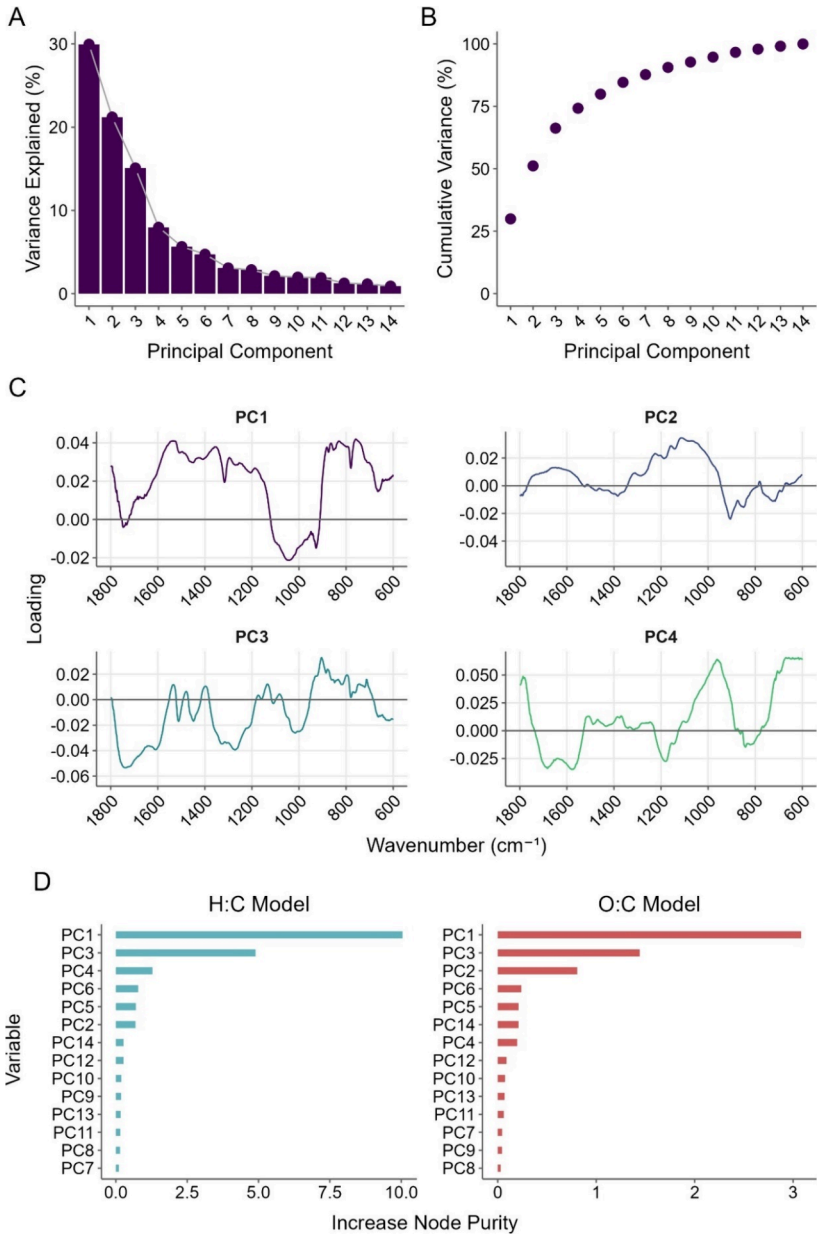

Figure 5. Exploration of PCA used in the preprocessing steps of model training. A) Scree plot showing variance explained of each individual PC, B) Cumulative variance of the principal components, C) Loadings of each wavenumber in the fingerprint region in the first 4 PCs, D) Variable importance of each PC for both the H:C and O:C model predictions as measured by increase in node purity, arranged in order of descending importance.

made with several lignocellulosic feedstocks. There are limited other studies that combine FTIR and modeling to predict biochar characteristics. Lago et al.[18] attained an R^2 of 0.81−0.87 for PLSR predictions of biochar cation exchange capacity from FTIR data using 18 feedstocks including non-lignocellulosic materials. De Morais and Silva[19] also used PLSR and FTIR to assess nutrient information on biochar-based fertilizers and achieved an $R^2 > 0.80$ for prediction of nitrogen pools. These relatively lower R^2 values are consistent with our PLSR results and may indicate that machine learning offers an advantage in place of simpler statistical models, or this could also be attributed to the wider variety of feedstocks in those studies. Zhu et al.[85] utilized RF models to predict carbon contents of lignocellulosic biochar based on known feedstock chemical composition and pyrolysis conditions and produced an R^2 of 0.76−0.85. The results of this study indicate that far simpler laboratory analyses in the form of FTIR can be performed to achieve more accurate predictions.

PCA Extraction and Variable Importance. RF_NSP was the best-performing model for both H:C and O:C predictions; it was thus the focus of the variable importance analysis. Variable importance helps identify the most influential predictors (i.e., specific wavenumbers) that drive the model's predictions. However, since PCA was used in preprocessing, PCs replaced individual wavenumbers. Figure 5 presents the PCA results, including the variance explained by each PC, spectral regions with high loadings, and the variable importance rankings for the best-performing model (RF_NSP) in predicting both molar ratios. Notably, the

https://doi.org/10.1021/acssusresmgt.5c00104
ACS Sustainable Resour. Manage. 2025, 2, 842−852

PCA was applied to the training data, which remained consistent for both H:C and O:C predictions.

In the scree plot in Figure 5A, the variance explained by the first four PCs are 30%, 21%, 15%, and 8% respectively, after which subsequent PCs individually contribute <7% of total variance. While the final model retained 14 PCs to reach 95% total variance, Figure 5B confirms that PCs 1-4 accounted for 74% of the cumulative variance. The gradual decay in explained variance suggests that the PCA preprocessing effectively reduced dimensionality for the original complex data. In Figure 5C, the loading values indicate the contribution of each wavenumber to that PC; however, because PCA is an unsupervised method, it is not possible to draw conclusions on the relationship between each PC and molar ratios with loadings information alone. PC1 had its highest positive loadings in the spectral regions of 1530 cm^{-1} (aromatic skeletal vibrations),[77] 1370 cm^{-1} (C−H symmetric deformation),[76] and 830−760 cm^{-1} (aromatic C−H bending and wagging).[69] PC1 therefore found signals associated with aromaticity most important in describing the data variance. PC1 had strong negative loadings in 1060−1000 cm^{-1} (C−O stretch of cellulose and lignin)[79] and 930 cm^{-1} (C−O−C ring vibration).[86] Samples with peaks in these regions reflect unpyrolyzed material still rich in lignin and cellulose, making them inversely correlated to the positive aromaticity loadings. PC2 was influenced strongly by positive loadings at 1100 cm^{-1} (asymmetric C−O−C stretch in cellulose)[74] and a negative loading at 900 cm^{-1} as seen similarly on PC1. PC3 was dominated by negative loadings in 1740−1550 cm^{-1} (carbonyl stretches)[76] and 1400−1200 cm^{-1} (C−H deformation moieties).[79] Lastly, the top positive loadings of PC4 included 1800 cm^{-1} (carboxyl groups),[87] 960 cm^{-1} (out-of-plane aromatic bending),[88] and 700−600 cm^{-1}, although the lower end of the spectrum could be attributable to a rising baseline caused by scattering.

The variable importance was assessed by the increase in node purity metric (IncNodePurity), which quantifies the ability of each predictor variable to separate the data into homogeneous subgroups.[89] IncNodePurity is a unitless measure reflecting the cumulative reduction in variance achieved by splitting that variable. Figure 5D reveals that for the H:C model, the top 3 important variables were PC1, PC3, and PC4 with IncNodePurity values of 10.04, 4.89, and 1.28, respectively, with other PCs having much lower importance. Therefore, PC1 creates the most meaningful and homogenous subdivisions in the data and is most important for prediction, aligning with PC1 capturing the most critical spectral information. Notably, PC2, which mostly represents the asymmetric stretch of C−O−C in cellulose, does not appear in top variables for predicting H:C ratios, meaning it contains less relevant information for predictions of H:C.[90] For the O:C model, PC1 again demonstrated the highest IncNodePurity of 3.08, indicating a substantial contribution to reducing variance and improving model accuracy. This was followed by PC3 and PC2, which had IncNodePurity = 1.44 and 0.80 respectively. Interestingly, PC3, while explaining only 8% of the variance in the data, was the second-most-important variable for both models. The lowest-ranked PCs have minimal contributions to predictive accuracy. This analysis demonstrates PCA's utility in data complexity reduction and the identification of the most predictive variables in the models. Sensitivity analyses linking varying numbers of PCs retained in model training to the interpretability of variable importance can be found in the Supporting Information.

Model Application. H:C and O:C molar ratios are industry-standard proxies for biochar stability, used by producers, buyers, and regulatory bodies. Certification bodies like the EBC require laboratory analysis for these ratios, which is a costly and time-consuming process. Purpose-built machine learning models can alleviate some of this burden by providing a real-time verification tool, potentially for on-site analysis. Biochar producers could also train their own FTIR models as a production monitoring measure. In field research, models could be integrated into handheld spectrometers, which provide accurate soil sample analyses,[91] to delivery instant stability predictions. Additionally, there is growing momentum in low- and middle-income countries producing "artisanal" biochar, often using off-grid kilns in rural areas.[92] These producers lack precise temperature controls and work with heterogeneous feedstocks, making quality assessment challenging. FTIR readings combined with machine learning could provide rapid stability insights without knowledge of production conditions.

However, as with all machine learning models, generalization remains a challenge, and the model performance may vary across different FTIR instruments. To address this, we recommend either centralized laboratory use or expanding training datasets to include diverse instrumentation. Moreover, this study focused exclusively on lignocellulosic feedstocks, and further research is needed to assess generalization to other materials. Given that FTIR is an information-rich technique, future studies could explore predicting other biochar properties that are directly linked to functional groups in the spectra such as proximate analysis outcomes. As biochar technology continues to evolve, advanced analytical tools such as the methods outlined here are essential for ensuring quality control and driving further innovation in the field.

CONCLUSIONS

This research investigated the prediction of biochar H:C and O:C molar ratios by training various machine learning models on FTIR spectral data. Expanding on previous studies, this work incorporated a diverse range of lignocellulosic feedstocks and evaluated models on an independent dataset comprising a previously unseen feedstock and HTTs. While the majority of models achieved R^2 > 0.9 on training data, performance declined on test data, highlighting limitations in generalization. RF models, when combined with normalization, scaling, and PCA preprocessing, were the most optimal for predicting biochar stability information from FTIR data (R^2_{test} = 0.96). Variable importance analysis determined that PC1, which captures spectral variance associated with aromaticity and C−O stretches in cellulose and lignin, was the most significant predictor for H:C and O:C. FTIR is already widely used in biochar research as a rapid and cost-effective qualitative method. This study demonstrates that when integrated with machine learning, FTIR data can be transformed into a powerful predictive tool for biochar stability.

ASSOCIATED CONTENT

Supporting Information

The Supporting Information is available free of charge at https://pubs.acs.org/doi/10.1021/acssusresmgt.5c00104.

FTIR data (XLSX)

https://doi.org/10.1021/acssusresmgt.5c00104
ACS Sustainable Resour. Manage. 2025, 2, 842−852

Elemental data, FTIR spectra (3700−2500 cm^{-1}), estimated biochar carbon storage, hyperparameter tuning, sensitivity analysis, and correlation plots between PC1 and other variables (PDF)

AUTHOR INFORMATION

Corresponding Author

Monica A. McCall − *Earth Science and Engineering, Imperial College London, London SW7 2AZ, United Kingdom; Grantham Institute for Climate Change and the Environment, Imperial College London, South Kensington, London SW7 2AZ, United Kingdom;* orcid.org/0009-0004-2598-3477; Email: monica.mccall@imperial.ac.uk

Authors

Jonathan S. Watson − *Earth Science and Engineering, Imperial College London, London SW7 2AZ, United Kingdom*

Jonathan S. W. Tan − *Earth Science and Engineering, Imperial College London, London SW7 2AZ, United Kingdom; Viridien Satellite Mapping, Crawley RH10 9QN, United Kingdom*

Mark A. Sephton − *Earth Science and Engineering, Imperial College London, London SW7 2AZ, United Kingdom*

Complete contact information is available at: https://pubs.acs.org/10.1021/acssusresmgt.5c00104

Notes

The authors declare no competing financial interest.

ACKNOWLEDGMENTS

This research was funded by a UK National Environment Research Council (NERC) CASE studentship supported by CO2CO Ltd, in conjunction with the Grantham Institute for Climate Change and the Environment. For the purpose of open access, the author has applied a 'Creative Commons Attribution' (CC BY) license to any Author Accepted Manuscript version arising.

REFERENCES

(1) Calvin, K.; Dasgupta, D.; Krinner, G.; Mukherji, A.; Thorne, P. W.; Trisos, C.; Romero, J.; Aldunce, P.; Barrett, K.; Blanco, G.; Cheung, W. W. L.; Connors, S.; Denton, F.; Diongue-Niang, A.; Dodman, D.; Garschagen, M.; Geden, O.; Hayward, B.; Jones, C.; Jotzo, F.; Krug, T.; Lasco, R.; Lee, Y.-Y.; Masson-Delmotte, V.; Meinshausen, M.; Mintenbeck, K.; Mokssit, A.; Otto, F. E. L.; Pathak, M.; Pirani, A.; Poloczanska, E.; Pörtner, H.-O.; Revi, A.; Roberts, D. C.; Roy, J.; Ruane, A. C.; Skea, J.; Shukla, P. R.; Slade, R.; Slangen, A.; Sokona, Y.; Sörensson, A. A.; Tignor, M.; Van Vuuren, D.; Wei, Y.-M.; Winkler, H.; Zhai, P.; Zommers, Z.; Hourcade, J.-C.; Johnson, F. X.; Pachauri, S.; Simpson, N. P.; Singh, C.; Thomas, A.; Totin, E.; Arias, P.; Bustamante, M.; Elgizouli, I.; Flato, G.; Howden, M.; Méndez-Vallejo, C.; Pereira, J. J.; Pichs-Madruga, R.; Rose, S. K.; Saheb, Y.; Sánchez Rodríguez, R.; Ürge-Vorsatz, D.; Xiao, C.; Yassaa, N.; Alegría, A.; Armour, K.; Bednar-Friedl, B.; Blok, K.; Cissé, G.; Dentener, F.; Eriksen, S.; Fischer, E.; Garner, G.; Guivarch, C.; Haasnoot, M.; Hansen, G.; Hauser, M.; Hawkins, E.; Hermans, T.; Kopp, R.; Leprince-Ringuet, N.; Lewis, J.; Ley, D.; Ludden, C.; Niamir, L.; Nicholls, Z.; Some, S.; Szopa, S.; Trewin, B.; Van Der Wijst, K.-I.; Winter, G.; Witting, M.; Birt, A.; Ha, M.; Romero, J.; Kim, J.; Haites, E. F.; Jung, Y.; Stavins, R.; Birt, A.; Ha, M.; Orendain, D. J. A.; Ignon, L.; Park, S.; Park, Y.; Reisinger, A.; Cammaramo, D.; Fischlin, A.; Fuglestvedt, J. S.; Hansen, G.; Ludden, C.; Masson-Delmotte, V.; Matthews, J. B. R.; Mintenbeck, K.; Pirani, A.; Poloczanska, E.; Leprince-Ringuet, N.; Péan, C. *IPCC, 2023: Climate Change 2023: Synthesis Report. Contribution of Working Groups I, II and III to the Sixth Assessment Report of the Intergovernmental Panel on Climate Change [Core Writing Team,* Lee, H., Romero, J., *(Eds.)]. IPCC,* Intergovernmental Panel on Climate Change (IPCC); *First,* Geneva, Switzerland, 2023. DOI: 10.59327/IPCC/AR6-9789291691647.

(2) *Biochar for Environmental Management: Science and Technology*; Lehmann, J., Joseph, S., Eds.; Earthscan: London ; Sterling, VA, 2009.

(3) Kurniawan, T. A.; Othman, M. H. D.; Liang, X.; Goh, H. H.; Gikas, P.; Chong, K.-K.; Chew, K. W. Challenges and Opportunities for Biochar to Promote Circular Economy and Carbon Neutrality. *Journal of Environmental Management* **2023**, *332*, No. 117429.

(4) Joseph, S.; Cowie, A. L.; Van Zwieten, L.; Bolan, N.; Budai, A.; Buss, W.; Cayuela, M. L.; Graber, E. R.; Ippolito, J. A.; Kuzyakov, Y.; Luo, Y.; Ok, Y. S.; Palansooriya, K. N.; Shepherd, J.; Stephens, S.; Weng, Z. H.; Lehmann, J. How Biochar Works, and When It Doesn't: A Review of Mechanisms Controlling Soil and Plant Responses to Biochar. *GCB Bioenergy* **2021**, *13* (11), 1731−1764.

(5) Bakshi, K.; Bakshi, K. Considerations for Artificial Intelligence and Machine Learning: Approaches and Use Cases. In *2018 IEEE Aerospace Conference; IEEE: Big Sky, MT*, 2018; pp 1−9. DOI: 10.1109/AERO.2018.8396488.

(6) Karpatne, A.; Ebert-Uphoff, I.; Ravela, S.; Babaie, H. A.; Kumar, V. Machine Learning for the Geosciences: Challenges and Opportunities. *IEEE Transactions on Knowledge and Data Engineering* **2019**, *31* (8), 1544−1554.

(7) Nguyen, V. G.; Sharma, P.; Ağbulut, Ü.; Le, H. S.; Truong, T. H.; Dzida, M.; Tran, M. H.; Le, H. C.; Tran, V. D. Machine Learning for the Management of Biochar Yield and Properties of Biomass Sources for Sustainable Energy. *Biofuels, Bioproducts and Biorefining* **2024**, *18* (2), 567−593.

(8) Goswami, L.; Kushwaha, A.; Kafle, S. R.; Kim, B.-S. Surface Modification of Biochar for Dye Removal from Wastewater. *Catalysts* **2022**, *12* (8), 817.

(9) Wang, W.; Chang, J.-S.; Lee, D.-J. Machine Learning Applications for Biochar Studies: A Mini-Review. *Bioresource Technology* **2024**, *394*, No. 130291.

(10) Yan, C.; Wang, X.; Xia, S.; Zhao, J. Mechanistic Insights into the Removal of As(III) and As(V) by Iron Modified Carbon Based Materials with the Aid of Machine Learning. *Chemosphere* **2023**, *321*, No. 138125.

(11) Li, H.; Ai, Z.; Yang, L.; Zhang, W.; Yang, Z.; Peng, H.; Leng, L. Machine Learning Assisted Predicting and Engineering Specific Surface Area and Total Pore Volume of Biochar. *Bioresource Technology* **2023**, *369*, No. 128417.

(12) Li, Y.; Gupta, R.; You, S. Machine Learning Assisted Prediction of Biochar Yield and Composition via Pyrolysis of Biomass. *Bioresource Technology* **2022**, *359*, No. 127511.

(13) Cao, H.; Milan, Y. J.; Mood, S. H.; Ayiania, M.; Zhang, S.; Gong, X.; Lora, E. E. S.; Yuan, Q.; Garcia-Perez, M. A Novel Elemental Composition Based Prediction Model for Biochar Aromaticity Derived from Machine Learning. *Artificial Intelligence in Agriculture* **2021**, *5*, 133−141.

(14) Farrukh, M. A. *Advanced Aspects of Spectroscopy*; BoD−Books on Demand, 2012.

(15) Pasieczna-Patkowska, S.; Madej, J. Comparison of Photoacoustic, Diffuse Reflectance, Attenuated Total Reflectance and Transmission Infrared Spectroscopy for the Study of Biochars. *Polish Journal of Chemical Technology* **2018**, *20* (4), 75−83.

(16) Santos, M. C. D.; Morais, C. L. M.; Lima, K. M. G. ATR-FTIR Spectroscopy for Virus Identification: A Powerful Alternative. *Biomedical Spectroscopy and Imaging* **2021**, *9* (3−4), 103−118.

(17) Wehrle, R.; Welp, G.; Pätzold, S. Total and Hot-Water Extractable Organic Carbon and Nitrogen in Organic Soil Amendments: Their Prediction Using Portable Mid-Infrared Spectroscopy with Support Vector Machines. *Agronomy* **2021**, *11* (4), 659.

(18) Lago, B. C.; Silva, C. A.; Melo, L. C. A.; Morais, E. G. D. Predicting Biochar Cation Exchange Capacity Using Fourier Trans-

form Infrared Spectroscopy Combined with Partial Least Square Regression. *Science of The Total Environment* **2021**, *794*, No. 148762.
(19) de Morais, E. G.; Silva, C. A. PLS Regression Coupled with FTIR Analysis as a Fast Tool to Assess Properties and Nutrient Pools of Biochar-Based Fertilizers. *Communications in Soil Science and Plant Analysis* **2024**, *55* (10), 1404−1419.
(20) Sajdak, M.; Kotyczka-Morańska, M. Development and Validation of a Fast Method Based on Infrared Spectroscopy for Biochar Quality Assessment. *Biomass and Bioenergy* **2018**, *112*, 99−109.
(21) Leng, L.; Huang, H.; Li, H.; Li, J.; Zhou, W. Biochar Stability Assessment Methods: A Review. *Science of The Total Environment* **2019**, *647*, 210−222.
(22) European Biochar Certificate - Guidelines for a Sustainable Production of Biochar, 2022. http://european-biochar.org.
(23) International Biochar Initiative (IBI). *Standardized Product Definition and Product Testing Guidelines for Biochar That Is Used in Soil, Version 2.0*; 2014.
(24) McCall, M. A.; Watson, J. S.; Sephton, M. A. Predicting Stability of Barley Straw-Derived Biochars Using Fourier Transform Infrared Spectroscopy. *ACS Sustainable Resour. Manage.* **2024**, *1*, 1975.
(25) Jayakumar, M.; Hamda, A. S.; Abo, L. D.; Daba, B. J.; Venkatesa Prabhu, S.; Rangaraju, M.; Jabesa, A.; Periyasamy, S.; Suresh, S.; Baskar, G. Comprehensive Review on Lignocellulosic Biomass Derived Biochar Production, Characterization, Utilization and Applications. *Chemosphere* **2023**, *345*, No. 140515.
(26) European Biochar Certificate. *Positive List of Permissible Biomasses for the Production of Biochar*, 2023. https://www.european-biochar.org/media/doc/2/positive-list_en_v10_3.pdf.
(27) Sun, R. C.; Sun, X. F.; Fowler, P.; Tomkinson, J. Structural and Physico-Chemical Characterization of Lignins Solubilized during Alkaline Peroxide Treatment of Barley Straw. *European Polymer Journal* **2002**, *38* (7), 1399−1407.
(28) Sun, X.-F.; Jing, Z.; Fowler, P.; Wu, Y.; Rajaratnam, M. Structural Characterization and Isolation of Lignin and Hemicelluloses from Barley Straw. *Industrial Crops and Products* **2011**, *33* (3), 588−598.
(29) Vargas, F.; González, Z.; Rojas, O. J.; Garrote, G.; Rodriguez, A. Barley Straw (Hordeum Vulgare) as a Supplementary Raw Material for Eucalyptus Camaldulensis and Pinus Sylvestris Kraft Pulp in the Paper Industry. *BioResources* **2015**, *10* (2), 3682−3693.
(30) Plazonić, I.; Barbarić-Mikočević, Ž.; Antonović, A. Chemical Composition of Straw as an Alternative Material to Wood Raw Material in Fibre Isolation. *Drvna ind.* **2016**, *67* (2), 119−125.
(31) Juárez, M.; Sánchez, R.; Espinosa, E.; Domínguez-Robles, J.; Bascón-Villegas, I.; Rodríguez, A. ENVIRONMENTALLY FRIENDLY LIGNOCELLULOSE NANOFIBRES FROM BARLEY STRAW. *Cellulose Chem. Technol.* **2018**, *52*, 589.
(32) Jackson, M. G. Review Article: The Alkali Treatment of Straws. *Animal Feed Science and Technology* **1977**, *2* (2), 105−130.
(33) Ludueña, L.; Fasce, D.; Alvarez, Vera. A.; Stefani, P. M. Nanocellulose from Rice Husk Following Alkaline Treatment to Remove Silica. *BioRes.* **2011**, *6* (2), 1440−1453.
(34) Kumar, S.; Sangwan, P.; Dhankar, R.; Mor, V.; Bidra, S. Utilization of Rice Husk and Their Ash: A Review. *Research Journal of Chemical and Environmental Sciences* **2013**, *1*, 126.
(35) Sreesvarna, B.; Subramanian, P.; Gitanjali, J.; Pugalendhi, S. Characterization of Rice Husk for Sustainable Applications. *Madras Agricultural Journal* **2019**, *106* (Spl), 279.
(36) Fengel, D.; Wegener, G. *Wood: Chemistry, Ultrastructure, Reactions*; de Gruyter: Berlin, 1989.
(37) Vinciguerra, V.; Spina, S.; Luna, M.; Petrucci, G.; Romagnoli, M. Structural Analysis of Lignin in Chestnut Wood by Pyrolysis-Gas Chromatography/Mass Spectrometry. *Journal of Analytical and Applied Pyrolysis* **2011**, *92* (2), 273−279.
(38) Zikeli, F.; Vinciguerra, V.; Taddei, A. R.; D'Annibale, A.; Romagnoli, M.; Mugnozza, G. S. Isolation and Characterization of Lignin from Beech Wood and Chestnut Sawdust for the Preparation of Lignin Nanoparticles (LNPs) from Wood Industry Side-Streams. *Holzforschung* **2018**, *72* (11), 961−972.
(39) Vázquez, G.; Fontenla, E.; Santos, J.; Freire, M. S.; González-Álvarez, J.; Antorrena, G. Antioxidant Activity and Phenolic Content of Chestnut (*Castanea Sativa*) Shell and Eucalyptus (*Eucalyptus Globulus*) Bark Extracts. *Industrial Crops and Products* **2008**, *28* (3), 279−285.
(40) Neiva, D. M.; Araújo, S.; Gominho, J.; Carneiro, A. de C.; Pereira, H. Potential of *Eucalyptus Globulus* Industrial Bark as a Biorefinery Feedstock: Chemical and Fuel Characterization. *Industrial Crops and Products* **2018**, *123*, 262−270.
(41) Liu, Y.; Shi, H.; Wang, Y.; Wen, J. Analysis of Chemical Components and Liquefaction Process of Eucalyptus Globulus Bark. *Applied Chemical Engineering* **2021**, *4* (2), 29−36.
(42) Miranda, I.; Gominho, J.; Mirra, I.; Pereira, H. Fractioning and Chemical Characterization of Barks of *Betula Pendula* and *Eucalyptus Globulus*. *Industrial Crops and Products* **2013**, *41*, 299−305.
(43) Fernandes, A.; Cruz-Lopes, L.; Dulyanska, Y.; Domingos, I.; Ferreira, J.; Evtuguin, D.; Esteves, B. Eco Valorization of Eucalyptus Globulus Bark and Branches through Liquefaction. *Applied Sciences* **2022**, *12* (8), 3775.
(44) Demirbaş, A. Effect of Lignin Content on Aqueous Liquefaction Products of Biomass. *Energy Conversion and Management* **2000**, *41* (15), 1601−1607.
(45) Pan, S.; Pu, Y.; Foston, M.; Ragauskas, A. J. Compositional Characterization and Pyrolysis of Loblolly Pine and Douglas-Fir Bark. *Bioenerg. Res.* **2013**, *6* (1), 24−34.
(46) Valentín, L.; Kluczek-Turpeinen, B.; Willför, S.; Hemming, J.; Hatakka, A.; Steffen, K.; Tuomela, M. Scots Pine (*Pinus Sylvestris*) Bark Composition and Degradation by Fungi: Potential Substrate for Bioremediation. *Bioresource Technology* **2010**, *101* (7), 2203−2209.
(47) Barros, D.; Fernandes, É.; Jesus, M.; Barros, L.; Alonso-Esteban, J. I.; Pires, P.; Vaz Velho, M. The Chemical Characterisation of the Maritime Pine Bark Cultivated in Northern Portugal. *Plants* **2023**, *12* (23), 3940.
(48) Boonmanumsin, P.; Treeboobpha, S.; Jeamjumnunja, K.; Luengnaruemitchai, A.; Chaisuwan, T.; Wongkasemjit, S. Release of Monomeric Sugars from *Miscanthus Sinensis* by Microwave-Assisted Ammonia and Phosphoric Acid Treatments. *Bioresource Technology* **2012**, *103* (1), 425−431.
(49) Lee, W.-C.; Kuan, W.-C. Miscanthus as Cellulosic Biomass for Bioethanol Production. *Biotechnology Journal* **2015**, *10* (6), 840−854.
(50) Schäfer, J.; Sattler, M.; Iqbal, Y.; Lewandowski, I.; Bunzel, M. Characterization of Miscanthus Cell Wall Polymers. *GCB Bioenergy* **2019**, *11* (1), 191−205.
(51) Menges, F. *Spectragryph - optical spectroscopy software*. Spectroscopy. http://spectragryph.com/ (accessed 2023-10-25).
(52) Kuhn, M. *Classification and Regression Training: The Caret Package*, 2019. https://topepo.github.io/caret/.
(53) Misra, P.; Yadav, A. S. Impact of Preprocessing Methods on Healthcare Predictions. *SSRN Journal* **2019**, DOI: 10.2139/ssrn.3349586.
(54) Tkachenko, Y.; Niedzielski, P. FTIR as a Method for Qualitative Assessment of Solid Samples in Geochemical Research: A Review. *Molecules* **2022**, *27* (24), 8846.
(55) Stone, M. Cross-Validatory Choice and Assessment of Statistical Predictions. *Journal of the Royal Statistical Society: Series B (Methodological)* **1974**, *36* (2), 111−133.
(56) Tougui, I.; Jilbab, A.; Mhamdi, J. E. Impact of the Choice of Cross-Validation Techniques on the Results of Machine Learning-Based Diagnostic Applications. *Healthc Inform Res.* **2021**, *27* (3), 189−199.
(57) Yang, L.; Shami, A. On Hyperparameter Optimization of Machine Learning Algorithms: Theory and Practice. *Neurocomputing* **2020**, *415*, 295−316.
(58) Zou, H.; Hastie, T. Regularization and Variable Selection Via the Elastic Net. *Journal of the Royal Statistical Society Series B: Statistical Methodology* **2005**, *67* (2), 301−320.

(59) Rigatti, S. J. Random Forest. *Journal of Insurance Medicine* **2017**, *47* (1), 31−39.
(60) Yu, H.; Kim, S. SVM Tutorial: Classification, Regression, and Ranking. *Handbook of Natural Computing* 2012; p 479.
(61) Aller, M. F. Biochar Properties: Transport, Fate, and Impact. *Critical Reviews in Environmental Science and Technology* **2016**, *46* (14−15), 1183−1296.
(62) Tag, A. T.; Duman, G.; Ucar, S.; Yanik, J. Effects of Feedstock Type and Pyrolysis Temperature on Potential Applications of Biochar. *Journal of Analytical and Applied Pyrolysis* **2016**, *120*, 200−206.
(63) International Biochar Initiative (IBI). *Biochar Classification Tool*. https://biochar-international.org/biochar-classification-tool-interface/ (accessed 2024-10-04).
(64) Ahmad Bhat, S.; Kuriqi, A.; Dar, M. U. D.; Bhat, O.; Sammen, S. Sh.; Towfiqul Islam, A. R. Md.; Elbeltagi, A.; Shah, O.; AI-Ansari, N.; Ali, R.; Heddam, S. Application of Biochar for Improving Physical, Chemical, and Hydrological Soil Properties: A Systematic Review. *Sustainability* **2022**, *14* (17), 11104.
(65) Ramírez-Estrada, A.; Mena-Cervantes, V. Y.; Mederos-Nieto, F. S.; Pineda-Flores, G.; Hernández-Altamirano, R. Assessment and Classification of Lignocellulosic Biomass Recalcitrance by Principal Components Analysis Based on Thermogravimetry and Infrared Spectroscopy. *Int. J. Environ. Sci. Technol.* **2022**, *19* (4), 2529−2544.
(66) Tatzber, M.; Stemmer, M.; Spiegel, H.; Katzlberger, C.; Zehetner, F.; Haberhauer, G.; Garcia Garcia, E.; Gerzabek, M. H. Spectroscopic Behaviour of 14C-Labeled Humic Acids in a Long-Term Field Experiment with Three Cropping Systems. *Aust. J. Soil Res.* **2009**, *47*, 459−469.
(67) Stefke, B.; Windeisen, E.; Schwanninger, M.; Hinterstoisser, B. Determination of the Weight Percentage Gain and of the Acetyl Group Content of Acetylated Wood by Means of Different Infrared Spectroscopic Methods. *Anal. Chem.* **2008**, *80* (4), 1272−1279.
(68) Shahrokh Abadi, M. H. Effects of Annealing Temperature on Infrared Spectra of SiO2 Extracted From Rice Husk. *Journal of Ceramic Science and Technology* **2014**, *5*, 1−5.
(69) Ibarra, JoséV.; Moliner, R.; Bonet, A. J. FT-i.r. Investigation on Char Formation during the Early Stages of Coal Pyrolysis. *Fuel* **1994**, *73* (6), 918−924.
(70) Chen, Y.; Zhang, X.; Chen, W.; Yang, H.; Chen, H. The Structure Evolution of Biochar from Biomass Pyrolysis and Its Correlation with Gas Pollutant Adsorption Performance. *Bioresource Technology* **2017**, *246*, 101−109.
(71) Grasel, F. D. S.; Ferrão, M. F.; Wolf, C. R. Development of Methodology for Identification the Nature of the Polyphenolic Extracts by FTIR Associated with Multivariate Analysis. *Spectrochimica Acta Part A: Molecular and Biomolecular Spectroscopy* **2016**, *153*, 94−101.
(72) Krysa, M.; Szymańska-Chargot, M.; Zdunek, A. FT-IR and FT-Raman Fingerprints of Flavonoids−A Review. *Food Chemistry* **2022**, *393*, No. 133430.
(73) Vázquez, G.; Antorrena, G.; González, J.; Freire, S. FTIR, 1H and 13C NMR Characterization of Acetosolv-Solubilized Pine and Eucalyptus Lignins. *Holzforschung* **1997**, *51* (2), 158−166.
(74) Pandey, K. K. A Study of Chemical Structure of Soft and Hardwood and Wood Polymers by FTIR Spectroscopy. *J. Appl. Polym. Sci.* **1999**, *71* (12), 1969−1975.
(75) Duca, D.; Pizzi, A.; Rossini, G.; Mengarelli, C.; Foppa Pedretti, E.; Mancini, M. Prediction of Hardwood and Softwood Contents in Blends of Wood Powders Using Mid-Infrared Spectroscopy. *Energy Fuels* **2016**, *30* (4), 3038−3044.
(76) Shah, M. A.; Khan, M. N. S.; Kumar, V. Biomass Residue Characterization for Their Potential Application as Biofuels. *J. Therm Anal Calorim* **2018**, *134* (3), 2137−2145.
(77) Rashid, T.; Kait, C. F.; Murugesan, T. A "Fourier Transformed Infrared" Compound Study of Lignin Recovered from a Formic Acid Process. *Procedia Engineering* **2016**, *148*, 1312−1319.
(78) Sammons, R. J.; Harper, D. P.; Labbé, N.; Bozell, J. J.; Elder, T.; Rials, T. G. Characterization of Organosolv Lignins Using Thermal and FT-IR Spectroscopic Analysis. *BioResources* **2013**, *8* (2), 2752−2767.
(79) Oh, S. Y.; Yoo, D. I.; Shin, Y.; Kim, H. C.; Kim, H. Y.; Chung, Y. S.; Park, W. H.; Youk, J. H. Crystalline Structure Analysis of Cellulose Treated with Sodium Hydroxide and Carbon Dioxide by Means of X-Ray Diffraction and FTIR Spectroscopy. *Carbohydrate Research* **2005**, *340* (15), 2376−2391.
(80) Ołdak, D.; Kaczmarek, H.; Buffeteau, T.; Sourisseau, C. Photo- and Bio-Degradation Processes in Polyethylene, Cellulose and Their Blends Studied by ATR-FTIR and Raman Spectroscopies. *J. Mater. Sci.* **2005**, *40* (16), 4189−4198.
(81) Solomon, P. R.; Carangelo, R. M. FT-i.r. Analysis of Coal. *Fuel* **1988**, *67* (7), 949−959.
(82) Tejado, A.; Peña, C.; Labidi, J.; Echeverria, J. M.; Mondragon, I. Physico-Chemical Characterization of Lignins from Different Sources for Use in Phenol−Formaldehyde Resin Synthesis. *Bioresource Technology* **2007**, *98* (8), 1655−1663.
(83) Injadat, M.; Moubayed, A.; Nassif, A. B.; Shami, A. Systematic Ensemble Model Selection Approach for Educational Data Mining. *Knowledge-Based Systems* **2020**, *200*, No. 105992.
(84) Montesinos López, O. A.; Montesinos López, A.; Crossa, J. Overfitting, Model Tuning, and Evaluation of Prediction Performance. In *Multivariate Statistical Machine Learning Methods for Genomic Prediction*; Springer International Publishing: Cham, 2022; pp 109−139. DOI: 10.1007/978-3-030-89010-0_4.
(85) Zhu, X.; Li, Y.; Wang, X. Machine Learning Prediction of Biochar Yield and Carbon Contents in Biochar Based on Biomass Characteristics and Pyrolysis Conditions. *Bioresource Technology* **2019**, *288*, No. 121527.
(86) Abdullah, A. H. D.; Chalimah, S.; Primadona, I.; Hanantyo, M. H. G. Physical and Chemical Properties of Corn, Cassava, and Potato Starchs. *IOP Conf. Ser.: Earth Environ. Sci.* **2018**, *160*, No. 012003.
(87) Younis, U.; Bokhari, T. Z.; Qayyum, M. F.; Malik, S. A.; Majeed, H.; Shah, M. H. R.; Tariq, A. Biochemical Characterization of Cotton Stalks Biochar Suggests Its Role in Soil as Amendment and Decontamination. *Advances in Environmental Research* **2017**, *6*, 127.
(88) Keiluweit, M.; Nico, P. S.; Johnson, M. G.; Kleber, M. Dynamic Molecular Structure of Plant Biomass-Derived Black Carbon (Biochar). *Environ. Sci. Technol.* **2010**, *44* (4), 1247−1253.
(89) Islam, K. I.; Elias, E.; Carroll, K. C.; Brown, C. Exploring Random Forest Machine Learning and Remote Sensing Data for Streamflow Prediction: An Alternative Approach to a Process-Based Hydrologic Modeling in a Snowmelt-Driven Watershed. *Remote Sensing* **2023**, *15* (16), 3999.
(90) Wei, L.; Ma, F.; Du, C. Application of FTIR-PAS in Rapid Assessment of Rice Quality under Climate Change Conditions. *Foods* **2021**, *10* (1), 159.
(91) Hutengs, C.; Ludwig, B.; Jung, A.; Eisele, A.; Vohland, M. Comparison of Portable and Bench-Top Spectrometers for Mid-Infrared Diffuse Reflectance Measurements of Soils. *Sensors* **2018**, *18* (4), 993.
(92) Namaswa, T.; Burslem, D. F. R. P.; Smith, J. Emerging Trends in Appropriate Kiln Designs for Small-Scale Biochar Production in Low to Middle Income Countries. *Bioresource Technology Reports* **2023**, *24*, No. 101641.